Photometric Data from Non-Resolved Objects for Space Object Characterization and Improved Atmospheric Modeling

Richard Linares*, Michael Shoemaker†, Andrew Walker‡, Piyush M. Mehta§, Brendt Wohlberg¶, David Palmer‖, David Thompson**, Josef Koller††, John L. Crassidis‡‡

1 Conference Paper

Accurate estimates for the drag coefficients of a satellite are important in reducing the biases in densities derived from satellite drag measurements as well as explicitly reducing the errors in orbit prediction. This develops a approach to estimate the drag coefficient for debris objects with known shape models.This paper focuses on rocket bodies in particular. The attitude and angular velocities are determined and there orientations estimates are used to computer the drag coefficient using a flat plate model. A nonlinear least squares estimator is used to estimate the attitude and angular velocity of the space object; both real data and simulated data scenarios are shown. A number representative rocket body models are used for simulated data examples, and real data examples. Good performance was shown for both simulated and real data case.

2 INTRODUCTION

The SSN network has the unique challenge of tracking more than 18,000 space objects (SOs) and providing critical collision avoidance warnings to military, NASA, and commercial systems. However, due to the large number of SOs and the limited number of sensors available to track them, it is impossible to maintain persistent surveillance. Observation gaps result in large propagation intervals between measurements and close approaches. Coupled with nonlinear SO dynamics this results in difficulty in modeling the probability distribution functions (pdfs) of the SO. In particular low-Earth orbiting (LEO) satellites are heavily influenced by atmospheric drag, which is very difficult to model accurately.

Los Alamos National Laboratory (LANL) has established a research effort, called IMPACT (Integrated Modeling of Perturbations in Atmospheres for Conjunction Tracking), to improve conjunction assessment via improved physics-based modeling. As part of this effort calibration satellite observations are used to dynamically calibrate the physics-based model and to improve its forecasting capability. The observations are collected from a variety of sources, including from LANL's own Raven-class optical telescope. This system collects both astrometric and photometric data on space objects. The photometric data will be used

*Graduate Student, Department of Mechanical and Aerospace Engineering, University at Buffalo, The State University of New York, Buffalo, NY 14260.

†Postdoctoral Research Associate, Space Science and Applications, ISR-1, Los Alamos National Laboratory, MS D466, Los Alamos, NM 87545.

‡Postdoctoral Research Associate, Space Science and Applications, ISR-1, Los Alamos National Laboratory, MS D466, Los Alamos, NM 87545.

§Graduate Research Assistant, Space Science and Applications, ISR-1, Los Alamos National Laboratory, MS D466, Los Alamos, NM 87545.

¶Senior Scientist, Theoretical Division, T-5, Los Alamos National Laboratory, MS D466, Los Alamos, NM 87545.

‖Senior Scientist, Space Science and Applications, ISR-3, Los Alamos National Laboratory, MS D466, Los Alamos, NM 87545.

**Senior Scientist (RULLI PI), Space Science and Applications, ISR-3, Los Alamos National Laboratory, MS D466, Los Alamos, NM 87545.

††Senior Scientist (IMPACT PI), Space Science and Applications, ISR-1, Los Alamos National Laboratory, MS D466, Los Alamos, NM 87545.

‡‡Professor, Department of Mechanical and Aerospace Engineering, University at Buffalo, The State University of New York, Buffalo, NY 14260.

to estimate the space objects' attitude and shape. This work uses measured photometric data from Los Alamos's own raven class telescope.

A number of atmospheric models exist which can be classified as either empirical or physics-based models. The current Air Force standard is the High Accuracy Satellite Drag Model (HASDM), which is an empirical model based on observation of calibration satellites . These satellite observations are used to determine model parameters based on their orbit determination solutions. Atmospheric orbits are perturbed by a number of factors including; drag coefficient, attitude, and shape of the space object. The satellites used for the HASDM model calibration process are chosen because of their relatively simple shapes, to minimize errors introduced due to shape miss-modeling. Under this requirement the number of calibration satellites that can be used for calibrating the atmospheric models is limited.

Simulations using computational methods produce accurate estimates for the drag coefficient, but are too slow for real-time applications of orbit prediction for conjunction assessment. Therefore, modeling the drag coefficient is very important. In this work, we present the technique for extracting drag coefficient from light curve measurements

Non-resolved photometric data have been studiedy by many as a mechanism for space object characterization. Photometry is the measurement of an object's flux or apparent brightness measured over a wavelength band. The temporal variation of photometric measurements is referred to as photometric signature. The photometric optical signature of an object contains information about shape, attitude, size and material composition. This work focuses on the processing of the data collected with LANL's telescope in an effort to use photometric data to expand the number of space objects that can be used as calibration satellites.

Light curves (the SO temporal brightness) have also been used to estimate the shape for an object. Light curve approaches have been studied to estimate the shape and state of asteroids. [1, 2] Reference [3] uses light curves and thermal emissions to recover the three-dimensional shape of an object assuming its orientation with respect to the observer is known. The benefits of using a light curve-based approach over the aforementioned others is that it is not limited to larger objects in lower orbits and it can be applied to small and dim objects in higher orbits, such as geosynchronous. Here light curve data is considered for shape estimation, which is useful because it provides a mechanism to estimate both position and attitude, as well as their respective rates. [4, 5]

In the realm of spacecraft dynamics and orbit determination, the drag coefficient is defined in three distinct ways: (i) a fixed drag coefficient, (ii) a fitted drag coefficient, and (iii) a physical drag coefficient. Fitted drag coefficients are estimated as part of an orbit determination process and fixed drag coefficients simply use a constant value for the drag coefficient. Errors from the use of fixed drag coefficients arise because of the application of the value of 2.2 derived for compact satellites [6] to satellites with complex geometries or geometries with high aspect ratio such as a rocket body. For high aspect ratio objects, there can be a large amount of shear that drastically increases the drag coefficient. Meanwhile, multiple reflections for complex geometries can also lead to divergence from the commonly used value of 2.2. The drag coefficient also changes with altitude and solar conditions. Fitted drag coefficients are specific to the atmospheric model used and therefore carry along the limitations of the atmospheric model and also frequently absorb other model errors. Physical drag coefficients are determined by the energy and momentum exchange of freestream atmospheric particles with the spacecraft surface3. Throughout this work, the term drag coefficients will refer to physical drag coefficients, unless stated otherwise.

The drag coefficient, characterized by the interaction between the atmosphere and the object, is an independent source of error whereas the errors in atmospheric mass density often stem from the use of fixed and/or fitted drag coefficients in its derivation from orbital drag measurements. Accurately deriving densities from drag measurements requires, in addition to accurate and high temporal resolution data (as in the case of an accelerometer), accurate modeling of the drag coefficient along the orbit. In addition, the use of fixed and/or fitted drag coefficients can by itself induce large orbit prediction errors.

Closed-form solutions for the drag coefficients of satellites with simple convex geometries like a sphere, cylinder, and cube in free molecular flow (FMF) were developed early in the Space Age [7, 8]; however, most satellites have complex shapes with concave geometries and require numerical modeling of the drag coefficient. The need for numerical modeling arises from multiple surface reflections and flow shadowing that changes the incident velocity distribution which is assumed to be Maxwellian for the analytic solutions. The drag coefficient in FMF is a function of the atmospheric translational temperature, T, surface temperature, T_w, spacecraft relative velocity, $\mathbf{v}_{\text{rel}}$, chemical composition of the atmosphere, and gas-surface interaction

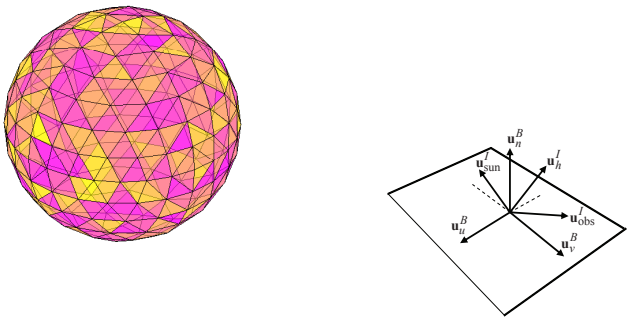

(a) Space Object Shape Model (b) Reflection Geometry

Figure 1: Reflection Geometry and Space Object Shape Model

(GSI) model.

The organization of this paper is as follows, first the methodology is briefly discussed, following this the shape model used in this work are discussed. Next light curve and flux calculate models are shown. Then atmospheric drag model is shown and the analytical expression for the flat plate C_D model is shown and discussed. Following this the nonlinear least squares approach using in this work is outlined. Finally, results are shown for simulated and real data examples discussions and conclusions are provided.

3 Shape Model Definition

The shape model considered in this work consists of a finite number a flat facets, where each facet has a set of basis vectors associated with it. These basis vectors are defined in Figure 1(b) and consist of three unit vectors $\mathbf{u}_n^B$, $\mathbf{u}_u^B$, and $\mathbf{u}_v^B$. The unit vector $\mathbf{u}_n^B$ points in the direction of the outward normal to the facet. For convex surfaces this model become more accurate as the number of facets are increased. The vectors $\mathbf{u}_u^B$ and $\mathbf{u}_v^B$ are in the plane of the facet. The space objects (SOs) are assumed to be rigid bodies and therefore the unit vectors $\mathbf{u}_n^B$, $\mathbf{u}_u^B$ and $\mathbf{u}_v^B$ do not change since they are expressed in the body frame.

The light curve and the solar radiation pressure (solar radiation pressure (SRP)) models discussed in the next sections require that these vectors be expressed in inertial coordinates and since the SO body is rotating, these vectors will change with respect to the inertial frame. The body vectors can be rotated to the inertial frame by the standard attitude mapping given by:

$$\mathbf{u}_i^B = A(\mathbf{q}_I^B)\mathbf{u}_k^I, \quad k = u,\, v,\, n \tag{1}$$

where $A(\mathbf{q}_I^B)$ is the attitude matrix mapping the inertial frame to the body frame using the quaternion parameterization. Furthermore, the unit vector $\mathbf{u}_{\text{sun}}^I$ points from the SO to the Sun direction and the unit vector $\mathbf{u}_{\text{obs}}^I$ points from the SO to the observer. The vector $\mathbf{u}_h^I$ is the normalized half vector between $\mathbf{u}_{\text{sun}}^I$ and $\mathbf{u}_{\text{obs}}^I$. This vector is also known as the Sun-SO-Observer bisector. Each facet has an area $\mathcal{A}(i)$ associated with it. Once the number of facets has been defined and their basis vectors are known, the areas $\mathcal{A}(i)$ define the size and shape of the SO. To determine the SRP forces and light curve characteristics, the surface properties must be defined for each facet.

Shape model used for this work used triangular facets defined by the location of their vertices $\mathbf{d}(i)$. Then the area of the i^{th} triangular facet formed by the convex hull of the control points is given by, $\mathcal{A}(i) = \|\mathbf{d}(i) \times \mathbf{l}(i)\|$, where $\mathbf{d}(i)$ and $\mathbf{l}(i)$ are the vectors defining the sides of the facets or $\mathbf{d}(i) = \mathbf{b}_i - \mathbf{b}_{i-1}$, $\mathbf{l}(i) = \mathbf{b}_i - \mathbf{b}_{i+1}$. The unit normal vector is given by

$$\mathbf{u}_n = \frac{\mathbf{d}(i) \times \mathbf{l}(i)}{\|\mathbf{d}(i) \times \mathbf{l}(i)\|} \tag{2}$$

For this work it is assumed that each facet has the same material parameters.

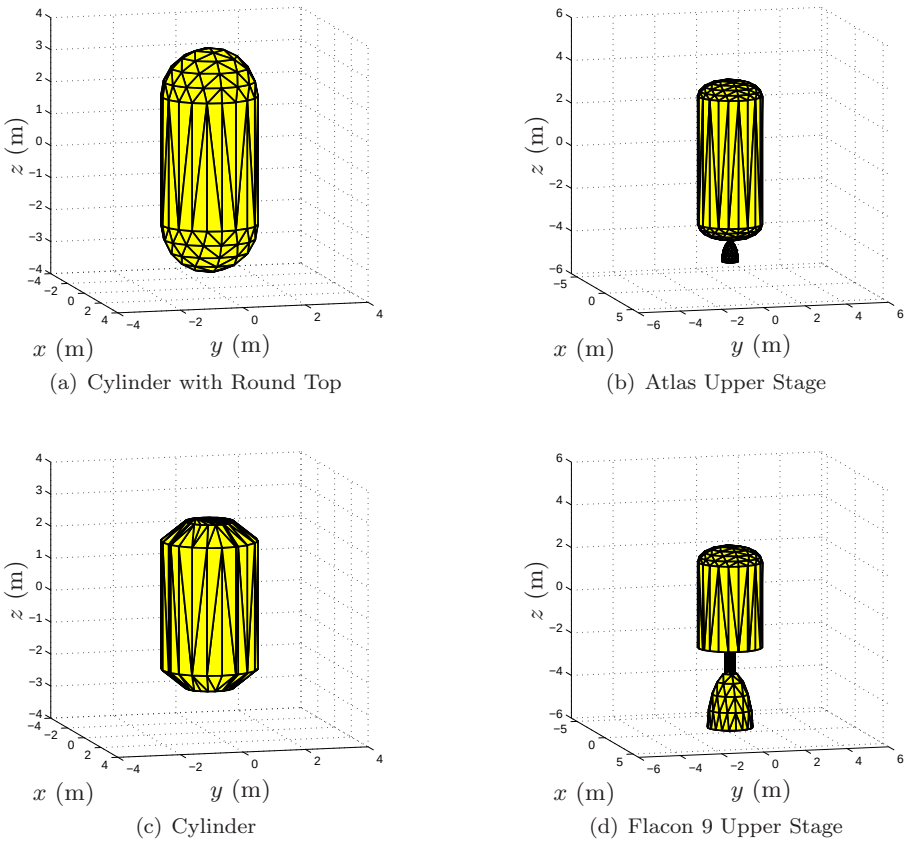

(a) Cylinder with Round Top

(b) Atlas Upper Stage

(c) Cylinder

(d) Flacon 9 Upper Stage

Figure 2: Representative Shape Models for Rocket Bodies

4 Ashikhmin-Shirley Model

In addition to the azimuth and elevation, the optical site also records the magnitude of the brightness of the SOs. The brightness of an object in space can be modeled using an anisotropic Phong light diffusion model. [9] This model is based on the bidirectional reflectance distribution function (BRDF) which models light distribution scattered from the surface due to the incident light. The BRDF at any point on the surface is a function of two directions, the direction from which the light source originates and the direction from which the scattered light leaves the observed the surface. The model in Ref. 9 decomposes the BRDF into a specular component and a diffuse component. The two terms sum to give the total BRDF:

$$\rho_{\text{total}}(i) = \rho_{\text{spec}}(i) + \rho_{\text{diff}}(i) \tag{3}$$

The diffuse component represents light that is scattered equally in all directions (Lambertian) and the specular component represents light that is concentrated about some direction (mirror-like). Reference 9 develops a model for continuous arbitrary surfaces but simplifies for flat surfaces. This simplified model is employed in this work as shape models are considered to consist of a finite number of flat facets. Therefore the total observed brightness of an object becomes the sum of the contribution from each facet.

Under the flat facet assumption the specular term of the BRDF becomes [9]

$$\rho_{\text{spec}}(i) = \frac{\sqrt{(n_u+1)\,(n_v+1)}}{8\pi} \frac{\left(\mathbf{u}_n^I(i)\cdot\mathbf{u}_h^I\right)^z}{\mathbf{u}_n^I(i)\cdot\mathbf{u}_{\text{sun}}^I + \mathbf{u}_n^I(i)\cdot\mathbf{u}_{\text{obs}}^I - (\mathbf{u}_n^I(i)\cdot\mathbf{u}_{\text{sun}}^I)(\mathbf{u}_n^I(i)\cdot\mathbf{u}_{\text{obs}}^I)} F_{\text{reflect}}(i) \tag{4}$$

where the exponent z is given by

$$z = \frac{n_u(\mathbf{u}_h^I\cdot\mathbf{u}_u^I(i))^2 + n_v(\mathbf{u}_h^I\cdot\mathbf{u}_v^I(i))^2}{(1-(\mathbf{u}_h^I\cdot\mathbf{u}_n^I(i))^2)} \tag{5}$$

where the Fresnel reflectance is given by

$$F_{\text{reflect}}(i) = R_{\text{spec}}(i) + (1 - R_{\text{spec}}(i)) \left(1 - \mathbf{u}^I_{\text{sun}} \cdot \mathbf{u}^I_h(i)\right)^5 \tag{6}$$

The parameters of the Phong model that dictate the direction (locally horizontal or vertical) distribution of the specular terms are n_u and n_v. The terms in Eq. (4) are functions of the reflection geometry which is described in Figure 1(b). The diffuse term of the BRDF is

$$\rho_{\text{diff}}(i) = \left(\frac{28 R_{\text{diff}}(i)}{23\pi}\right)(1 - R_{\text{spec}}(i)) \left[1 - \left(1 - \frac{\mathbf{u}^I_n(i) \cdot \mathbf{u}^I_{\text{sun}}}{2}\right)^5\right] \left[1 - \left(1 - \frac{\mathbf{u}^I_n(i) \cdot \mathbf{u}^I_{\text{obs}}}{2}\right)^5\right] \tag{7}$$

4.1 Flux Calculation

The apparent magnitude of an SOs is the result of sunlight reflecting off of its surfaces along the line-of-sight to an observer. First, the fraction of visible sunlight that strikes an object (and not absorbed) is computed by

$$F_{\text{sun}}(i) = C_{\text{sun,vis}}\, \rho_{\text{total}}(i) \left(\mathbf{u}^I_n(i) \cdot \mathbf{u}^I_{\text{sun}}\right) \tag{8}$$

where $C_{\text{sun,vis}} = 455$ W/m^2 is the power per square meter impinging on a given object due to visible light striking the surface. If either the angle between the surface normal and the observer's direction or the angle between the surface normal and Sun direction is greater than $\pi/2$ then there is no light reflected toward the observer. If this is the case then the fraction of visible light is set to $F_{\text{sun}}(i) = 0$. Next, the fraction of sunlight that strikes an object that is reflected must be computed:

$$F_{\text{obs}}(i) = \frac{F_{\text{sun}}(i)\mathcal{A}(i) \left(\mathbf{u}^I_n(i) \cdot \mathbf{u}^I_{\text{obs}}\right)}{\|\mathbf{d}^I\|^2} \tag{9}$$

The reflected light is now used to compute the apparent brightness magnitude, which is measured by an observer:

$$m_{\text{app}} = -26.7 - 2.5\log_{10}\left|\sum_{i=1}^{N} \frac{F_{\text{obs}}(i)}{C_{\text{sun,vis}}}\right| \tag{10}$$

where -26.7 is the apparent magnitude of the sun. The reflected light of each facet is now used to compute the total photon flux, which is measured by an observer:

$$\tilde{F} = \left[\sum_{i=1}^{N} F_{\text{obs}}(i)\right] + v_{\text{CDD}} \tag{11}$$

where v_{CDD} is the measurement noise associated with flux measured by a CCD sensor.

5 Atmospheric Drag

The drag acceleration on a satellite is defined by

$$\mathbf{a}^I_{\text{Drag}} = -\frac{1}{2}\frac{C_D \mathcal{A}}{m} \rho \mathbf{v}^2_{rel} \frac{\mathbf{v}_{rel}}{|\mathbf{v}_{rel}|} \tag{12}$$

where $\mathbf{a}^I_{\text{Drag}}$ is the drag force on the satellite, ρ is the mass density of the local atmosphere, $\mathbf{v}_{rel}$ is the relative velocity between the satellite and the co-rotating atmosphere, C_D is the satellite drag coefficient, A is the projected area of the satellite normal to the velocity vector, and m is the satellite mass. In practice, $\mathcal{A}$ and m are well-known for attitude-stabilized artificial satellites while $\mathbf{v}_{rel}$ can be assumed to be accurately known in the absence of atmospheric winds.

The remaining two unknowns are T and C_D. For orbital propagation, T is generally taken from an empirical atmospheric model such as NRLMSISE-00. This leaves C_D as the only remaining unknown parameter. Early in the space age, it was common practice to simply orbital propagation by using C_D 2.2; however, theoretical work has shown that C_D can have large variations away from the constant value of 2.2. C_D is

dependent on the atmospheric translation temperature, the speed of the satellite relative to the atmosphere, the satellite surface temperature, the atmospheric composition, the satellite surface composition, and the momentum and energy accommodation coefficients of the satellite surface.

Nearly all low Earth orbit satellites orbit at altitudes above 200 km where the atmosphere is free molecular. In free molecular flow, collisions between particles are so infrequent that they can be neglected. Under such conditions, closed-form solutions can be found for simple convex satellite geometries such as a sphere, flat plate, and cylinder. Closed-form solutions only exist for convex geometries because the concave geometries allow multiple reflections from the satellite surface and break a fundamental assumption of the solution that the incident velocity distribution function is Maxwellian.

The closed-form solution for the drag coefficient of a flat plate with a single side exposed to the flow is especially useful because any arbitrary geometry (convex or concave) can be decomposed into small flat plate elements. The total drag coefficient for the arbitrary geometry is then approximated as the sum of the drag coefficients of each of the flat plate elements. For convex geometries, the approximation converges to the true drag coefficient as the flat plate elements' size goes to zero. For concave geometries, the approximation does not account for multiple reflections from the satellite surface and is generally in error by a few percent.

Sentman [8] derived the closed-form solution for a flat plate with a single side exposed to the flow under the assumption of diffuse reflection. The solution in terms of the angle of attack, θ, is given by

$$\begin{aligned} C_D = &\cos(\theta)\left(1+\frac{1}{2s^2}\right)\left[1+\operatorname{erf}(s+\cos^2(\theta))\right] + \left(\frac{1}{\sqrt{\pi}s}+\frac{\cos^2(\theta)}{2s^2}\right)\exp\left\{(-s^2+\cos^2(\theta))\right\} \\ &+\sqrt{\frac{T_{(k,r)}}{T_s}}\left[\frac{\sqrt{\pi}}{2s}\cos^2(\theta)\left(1+\operatorname{erf}(s^2+\cos^2(\theta))\right)\right] \end{aligned} \tag{13}$$

The angle of attack is defined $\theta = \arccos(\mathbf{v}_{rel}^T \mathbf{u}_n)$. Here s is the speed ratio defined by

$$s = \frac{|\mathbf{v}_{rel}|}{v_{mp}} \tag{14}$$

where v_{mp} is the most probable speed of a Maxwellian velocity distribution at the local translational temperature of the atmosphere, T_∞, and is defined by

$$v_{mp} = \sqrt{\frac{2k_B T_\infty}{m_p}} \tag{15}$$

Here k_B is the Boltzmann constant and m_p is the atmospheric particle mass. The error function, $\operatorname{erf}(x)$, is defined as

$$\operatorname{erf}(x) = \frac{2}{\sqrt{\pi}}\int_0^x e^{-t^2}dt \tag{16}$$

$T_{(k,r)}$ is the kinetic reflected temperature and is defined by

$$T_{(k,r)} = T_{(k,i)}(1-\alpha) + \alpha T_s \tag{17}$$

where t is the energy accommodation coefficient and $T_{(k,i)}$ is the kinetic incident temperature defined by

$$T_{(k,i)} = \frac{m_p|\mathbf{v}_{rel}|^2}{3k_B} \tag{18}$$

When computing the drag coefficient for a mixture of gases, the total drag coefficient is the sum of the individual species drag coefficients weighted by the species mole fraction and particle mass and normalized by the average mass of the mixture, m_{avg}:

$$C_{(D,T)} = \frac{1}{m_{\text{avg}}}\sum_{j=i}^{N}\chi_j m_j C_{D,j} \tag{19}$$

Here N is the total number of species and m_{avg} is computed from

$$m_{\text{avg}} = \sum_{j=i}^{N}\chi_j m_j \tag{20}$$

6 Nonlinear Least Squares

The estimation approach choose for this work is the Nonlinear Least Squares (NLSQ) method. This method is a batch method and therefore it processes all the data at once. To apply the NLSQ method to attitude and angular velocity determination one much linear both the measurement and dynamic model. Also the attitude representation chose for this work is the quaternion and therefor the attitude error must be approximated by a small angle error to avoid the quaternion unit constraint. The goal is to estimate a state $\mathbf{x}_k$ for times t_k from measurements $\mathbf{z}_k$ for $k = 1, \ldots, m$. Consider the following dynamic and measurement model, assuming m scalar measurements with uncorrelated measurement errors

$$\mathbf{x}_{k+1} = \mathbf{f}_k(\mathbf{x}_k) \tag{21a}$$

$$\mathbf{z}_k = \mathbf{g}_k(\mathbf{x}_k) + \mathbf{n}_k \tag{21b}$$

where $\mathbf{n}_i \sim \mathcal{N}(\mathbf{n}_i; 0, \Sigma_i^2)$ and $E\{\mathbf{n}_i \mathbf{n}_j\} = \delta_{ij}\Sigma_i^2$. Then Eq. (21a) and Eq. (21a) can be used to estimate the initial condition of system, $\mathbf{x}_0$, by writing the measurements as $\mathbf{z}_k = \mathbf{g}_k(\phi_k(\mathbf{x}_0)) + \mathbf{n}_k$ where $\phi_k(\cdot)$ takes initial conditions and maps them to time k. The measurements can be written in vector form as

$$\mathbf{y} = \mathbf{h}(\mathbf{x}_0) + \mathbf{v} \tag{22}$$

where $\mathbf{y} = [\mathbf{z}_1, \ldots, \mathbf{z}_m]$, $\mathbf{v} \sim \mathcal{N}(\mathbf{v}; \mathbf{0}, R)$, $R = \text{diag}\left(\Sigma_1^2, \ldots, \Sigma_m^2\right)$, and $\mathbf{h}(\cdot) = \mathbf{g}_k(\phi_k(\cdot))$. The system in Eq (21) can be solved using nonlinear least square by linearizing the system about the current estimate. Using Taylor series expansion the measurement function from Eq. (22) can be written as

$$\mathbf{h}(\mathbf{x}_o) = \mathbf{h}(\hat{\mathbf{x}}_o) + H(\hat{\mathbf{x}}_o)(\hat{\mathbf{x}}_o - \mathbf{x}_o) + \mathcal{O}(2) \tag{23}$$

where $H = \frac{\partial \mathbf{h}(\hat{\mathbf{x}}_o)}{\partial \mathbf{x}_o}\Big|_{\mathbf{x}_o = \hat{\mathbf{x}}_o} = \frac{\partial \mathbf{g}(\phi_k(\hat{\mathbf{x}}_o))}{\partial \phi_k} \frac{\partial \phi_k(\hat{\mathbf{x}}_o)}{\partial \mathbf{x}_o}\Big|_{\mathbf{x}_o = \hat{\mathbf{x}}_o}$. The derivatives of the measurement function $\mathbf{g}(\cdot)$ and the dynamic function $\phi_k(\cdot)$ must be calculated. The derivatives of $\mathbf{g}_k(\cdot)$ can be derive from the equations in section §4 and where shown in reference **?**. The derivatives of $\phi_k(\cdot)$ involve the linearization of attitude kinematics and dynamic equations and these equations are shown later in the appendix. The NLSQ solution can be found by minimizing the following cost function

$$J(\mathbf{x}_o) = \frac{1}{2}\left[\mathbf{z} - \mathbf{h}(\mathbf{x}_i)\right]^T W \left[\mathbf{z} - \mathbf{h}(\mathbf{x}_i)\right] \tag{24}$$

where the weighting matrix is selected to be measurement covariance $W = R^{-1}$. The formal NLSQ iterative solution can be written as

$$\hat{\mathbf{x}}_o^{i+1} = \hat{\mathbf{x}}_o^i + \left[H_i^T W H_i\right]^{-1} H_i^T W [\mathbf{z} - \mathbf{h}(\mathbf{x}_i)] \tag{25}$$

where $P_o = E\{(\hat{\mathbf{x}}_o - \mathbf{x}_o)(\hat{\mathbf{x}}_o - \mathbf{x}_o)^T\}$ and $P_o = \left(H_i^T W H_i\right)^{-1}$ The estimate of $\mathbf{x}_o$ is obtained using Eq.(26) iteratively until a termination condition is met. Two conditions are set in this work, max number of iterations, $i_{\max}$, and relative tolerance

$$\epsilon = \frac{\|\hat{\mathbf{x}}_o^{i+1} - \hat{\mathbf{x}}_o^i\|}{\|\hat{\mathbf{x}}_o^i\|} \tag{26}$$

For this work $\epsilon = 0.1$ and $i_{\max} = 200$. This solution allows for a covariance to be computed for each time step by using P_o and the linearized dynamic equations. Then this covariance could be used to represent uncertainty in C_D that is computed from the orientation estimates.

7 SIMULATION RESULTS

This section discussed simulation results for the proposed method. Four examples are considered were for each example a different shape model is used. The shape models used are shown in Figure 2 were a cylinder with round top (Figure 2(a)), Atlas upper stage (Figure 2(b)), cylinder (Figure 2(c)), and a Flacon 9 upper stage (Figure 2(d)) models are used. Each model uses the same initial attitude and positions states and simulation conditions are given by

- Geographic position of the ground site is 0° North, 172° West with 0 km altitude

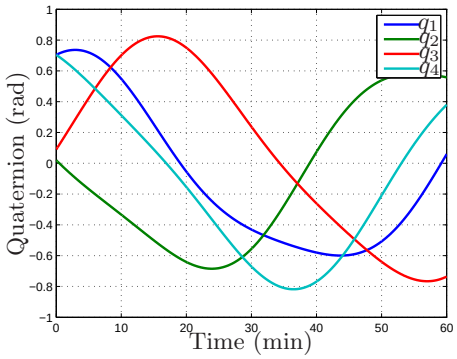

(a) Attitude (Deg)

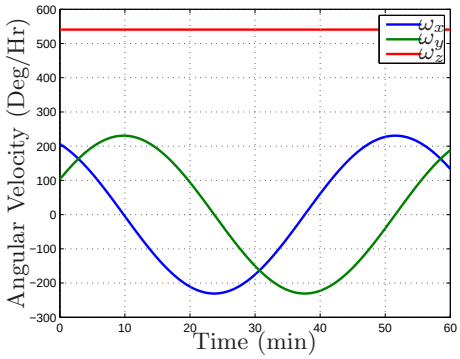

(b) Velocity Error (Deg/Hr)

Figure 3: True Attitude and Angular Velocity Profile

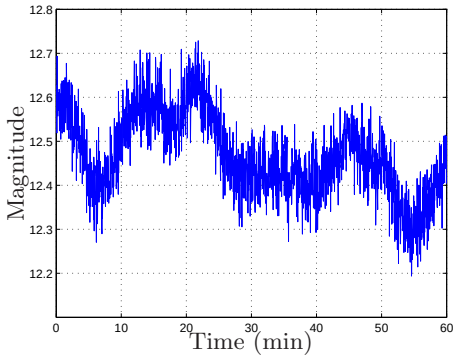

(a) Cylinder

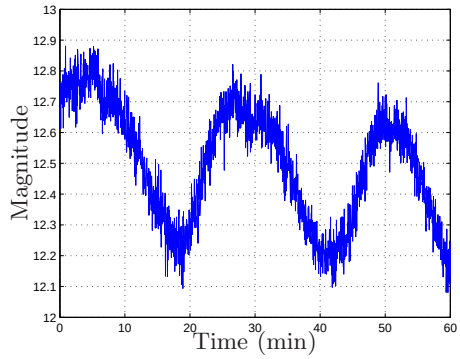

(b) Cylinder with Round Top

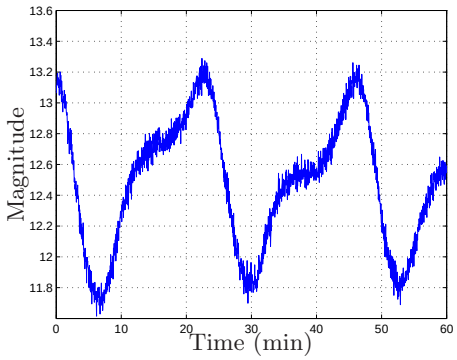

(c) Flacon 9 Upper Stage

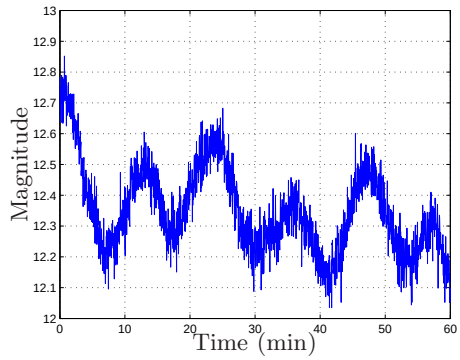

(d) Atlas Upper Stage

Figure 4: Magnitude for Different Rocket Body Models

- Initial inertial position and velocity are chosen as $\mathbf{r}^I = [-7.8931 \times 10^2 \;\; 3.6679 \times 10^4 \;\; 2.1184 \times 10^4]^T$ km
- Initial inertial velocity is chosen as $\mathbf{v}^I = [-3.0669 \;\; -4.9425 \times 10^{-2} \;\; -2.8545 \times 10^{-2}]^T$ km/s
- The initial time of the simulation is May 8, 2007 at 5:27.55
- Initial quaternion: $\mathbf{q}_I^B = [1/\sqrt{2} \;\; 0 \;\; 0 \;\; 1/\sqrt{2}]^T$
- A constant rotation rate, defined as the body rate with respect to the inertial frame, represented in body coordinates, is used given by $\boldsymbol{\omega}_{B/I}^B = [0 \;\; 0.00262 \;\; 0]^T$ rad/s

For all simulations scenarios, measurements are produced using zero-mean white-noise error processes with standard deviation of 0.05 for magnitude and standard deviation of 1 arc-seconds for azimuth and elevation. The initial errors for the states are 50 deg for all three attitudes, $1,000$ deg/hr for the rotational rate. The time interval between the measurements is set to 2 seconds. Data is simulated for 1 hours. The simulation true quaternion and angular velocity are shown in Figure 3 and simulation case had the same true orientational trajectories.

The orientational state estimates can be found the NLSQ approach for each case are shown in Figures 5, 6, 8, and 7. Figure 4 shows the simulated magnitude measurements for the models considered for this work. From this figure we can see that the simulate magnitude differ greatly for each rocket body model. The simple cylinder model has the smallest variation since it has the smallest number of shape feature and smoother shape. The Flacon 9 upper stage has the greatest variation since it has a very large nozzle which provides a district feature in the light curve. The cylinder with round top model and atlas upper stage of light curves of similar magnitudes but the atlas upper stage has additional variation due to the small nozzle in its shape model. We can see from the simulation results that all the model shown good performance in terms of the measurement residual and by how well the predicted observation match the actual observation. However, since the light curve for the model are different they do not show the same observability it terms of the attitude and angular velocity estimated. From Figure 8 we can see that Flacon 9 rocket body shows the best attitude error of about 0.2 Degs, 0.2 Degs, and 5 Degs, in Roll, Pitch, and Yaw respectively.

Finally, the estimates from the NLSQ approach are used to compute C_D using the equations from §5. These C_Ds are shown in Figure 9 for each rocket body model from this figure one can see that both variations due to rotation of the rocket bodies and variation due to changes of $\mathbf{v}_{\text{rel}}$ due to orbital motion. The C_D values can be used to compute a mean C_D and a variance about that mean. This could be used to quantify the uncertainty in C_D if one assume a constant C_D. These values could be used in an orbit propagation and orbit determination directly.

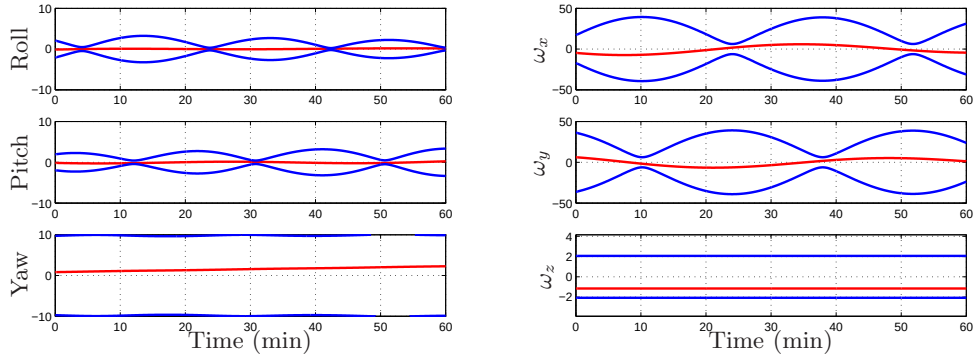

(a) Attitude (Deg)

(b) Velocity Error (Deg/Hr)

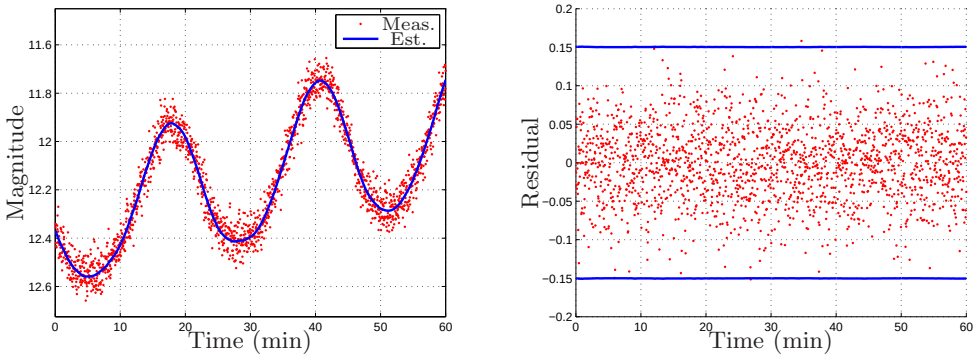

(c) Measured and Estimated Magnitude

(d) Residual

Figure 5: NLSQ Results for Cylinder with Round Top Rocket Body Model

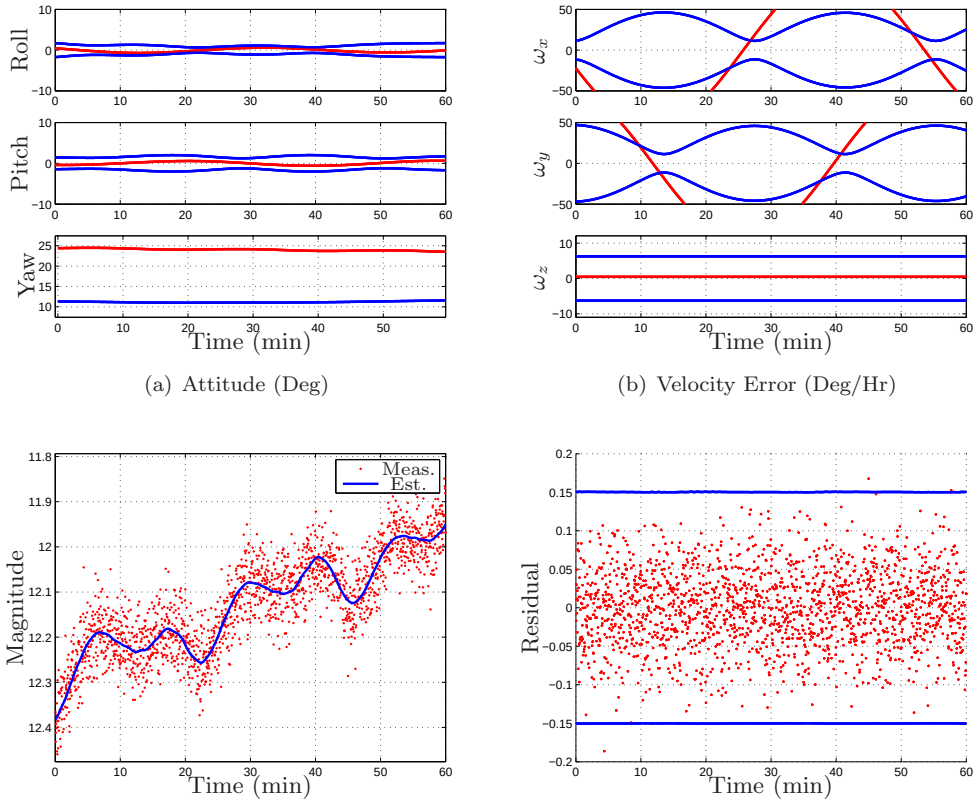

(a) Attitude (Deg)

(b) Velocity Error (Deg/Hr)

(c) Measured and Estimated Magnitude

(d) Residual

Figure 6: NLSQ Results for Cylinder Rocket Body Model

8 Actual Data Scenario

In this section actual data from Los Alamos's satellite observation campaign was used. The data use in this example was gathered September 19 2012 03:29:29.5 UT. The object that was observed was a ARIANE 3 Rocket body with SSN number 15562. The observation were made from a small raven class telescope. The observations were sample every second for 5 mins and the observations were taken from New Mexico. The simulation results for the real data example are shown in Figure 10. From Figure 10(c) we can see that predicted magnitude fits the observations well and captures the main period of the light curve measurements. The estimated quaternion and angular velocity are shown in Figures 10(a) and 10(b). The orientation trajectory was recovered from actual data but more development is required until this can provide an improvement orbit propagation, determination, or atmospheric density recovery. The measurement errors must be understood better to allow for actuate uncertainty quantification.

9 CONCLUSIONS

In this paper, an Nonlinear Least Squares estimation scheme using light curve measurements was presented and was used to estimate attitude and angular velocity of a space object (SO) along. The shape of the SO was assumed known and this work focused on rocket body with perigee lower then 300 km. The shape model used consisted of triangular facets to allow for the modeling of complex rocket body shapes. Four different rocket body models were used that included, a simple cylinder, a simple cylinder with rounded top, a Flacon 9 upper stage, and an Atlas upper stage. The light curve model used was based on the Ashikhmin-Shirley BRDF and showed good performance for simulated and real data examples. The estimated orientation trajectories were used to estimate the drag coefficient of the SO over an orbit. This drag coefficient can then be used in orbit determination, orbit propagation, or to bound uncertainty of the drag coefficient over

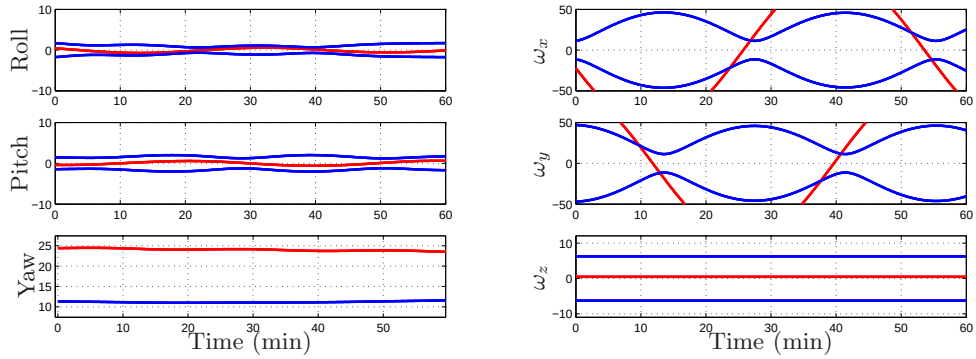

(a) Attitude (Deg)

(b) Velocity Error (Deg/Hr)

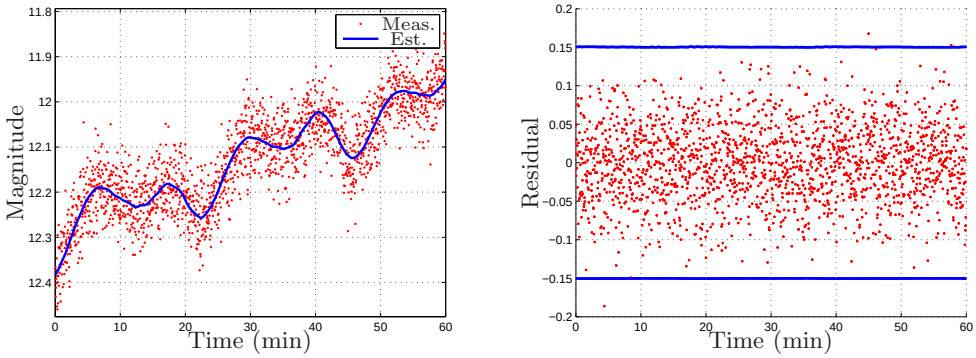

(c) Measured and Estimated Magnitude

(d) Residual

Figure 7: NLSQ Results for Altas Rocket Body Model

the orbit based on orientation variations. Future work will study the use of this approach along with the Tomography method to recover density.

10 Appendix

In terms of the quaternion, the attitude matrix is given by

$$A(\mathbf{q}) = \Xi^T(\mathbf{q})\Psi(\mathbf{q}) \tag{27}$$

where

$$\Xi(\mathbf{q}) \equiv \begin{bmatrix} q_4 I_{3\times 3} + [\boldsymbol{\varrho}\times] \\ -\boldsymbol{\varrho}^T \end{bmatrix} \tag{28a}$$

$$\Psi(\mathbf{q}) \equiv \begin{bmatrix} q_4 I_{3\times 3} - [\boldsymbol{\varrho}\times] \\ -\boldsymbol{\varrho}^T \end{bmatrix} \tag{28b}$$

with

$$[\mathbf{a}\times] \equiv \begin{bmatrix} 0 & -a_3 & a_2 \\ a_3 & 0 & -a_1 \\ -a_2 & a_1 & 0 \end{bmatrix} \tag{29}$$

for any general 3×1 vector $\mathbf{a}$ defined such that $[\mathbf{a}\times]\mathbf{b} = \mathbf{a} \times \mathbf{b}$. This representation is constrained since the quaternion is of unit length and therefore $\mathbf{q}^T\mathbf{q} = 1$. The kinematics dynamics are given by a first-order

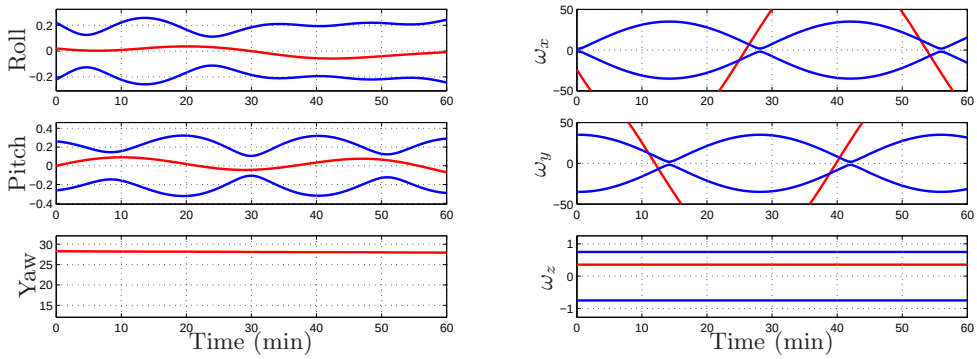

(a) Attitude (Deg)

(b) Velocity Error (Deg/Hr)

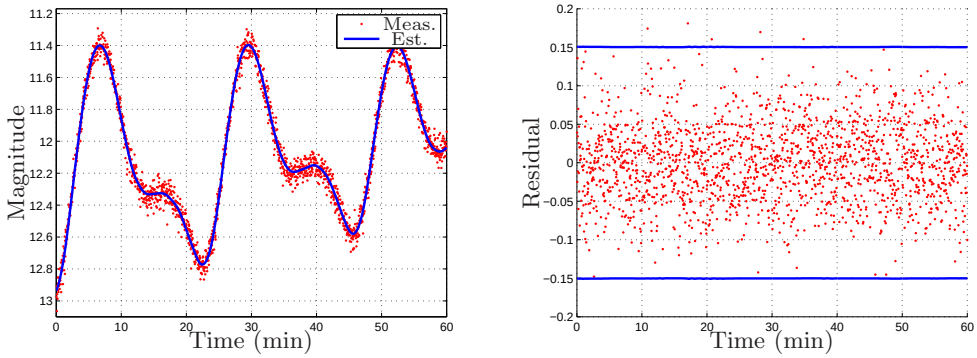

(c) Measured and Estimated Magnitude

(d) Residual

Figure 8: NLSQ Results for Flacon 9 Rocket Body Model

differential equation:

$$\dot{\mathbf{q}} = \frac{1}{2}\Xi(\mathbf{q})\boldsymbol{\omega} \tag{30a}$$

$$\dot{\boldsymbol{\omega}}^B_{B/I} = J_{\mathrm{SO}}^{-1}\left(\mathbf{T}^B_{\mathrm{srp}} - \left[\boldsymbol{\omega}^B_{B/I}\times\right] J_{\mathrm{SO}}\boldsymbol{\omega}^B_{B/I}\right) \tag{30b}$$

11 Acknoledgement

The authors gratefully acknowledge the support of the U.S. Department of Energy through the LANL/LDRD Program for this work.

References

[1] Kaasalainen, M. and Torppa, J., "Optimization Methods for Asteriod Lightcurve Inversion I: Shape Determination," *Icarus*, Vol. 153, No. 4, Jan. 2001, pp. 24–36.

[2] Kaasalainen, M. and Torppa, J., "Optimization Methods for Asteriod Lightcurve Inversion II: The Complete Inverse Problem," *Icarus*, Vol. 153, No. 4, Jan. 2001, pp. 37–51.

[3] Calef, B., Africano, J., Birge, B., Hall, D., and Kervin, P. W., "Photometric Signature Inversion," *Proceedings of the International Society for Optical Engineering*, Vol. 6307, San Diego, CA, Aug. 2006, Paper 11.

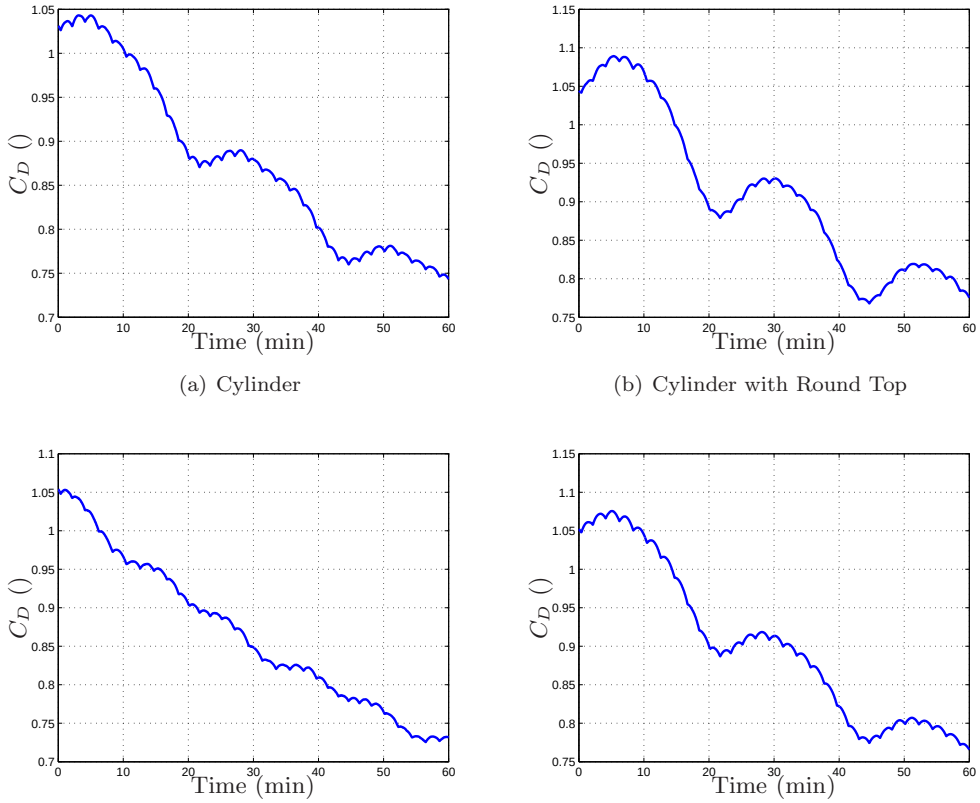

(a) Cylinder

(b) Cylinder with Round Top

(c) Flacon 9 Upper Stage

(d) Atlas Upper Stage

Figure 9: Drag Coefficient For Different Rocket Body Models

[4] Jah, M. and Madler, R., "Satellite Characterization: Angles and Light Curve Data Fusion for Spacecraft State and Parameter Estimation," *Proceedings of the Advanced Maui Optical and Space Surveillance Technologies Conference*, Vol. 49, Wailea, Maui, HI, Sept. 2007, Paper E49.

[5] Centinello, F. J., "Six Degree of Freedom Estimation with Light Curve Data," Tech. rep., Air Force Research Laboratory, Kihei, HI, 2008.

[6] Cook, G. E., "Satellite drag coefficients," *planss*, Vol. 13, Oct. 1965, pp. 929.

[7] Schaaf, S. A. and Chambré, P. L., *Flow of rarefied gases*, Princeton University Press Princeton, 1961.

[8] Sentman, L., Missiles, L., and Company, S., *Free Molecule Flow Theory and Its Application to the Determination of Aerodynamic Forces*, LMSC-448514, Lockheed Missiles & Space Company, a division of Lockheed Aircraft Corporation, 1961.

[9] Ashikmin, M. and Shirley, P., "An Anisotropic Phong Light Reflection Model," Tech. Rep. UUCS-00-014, University of Utah, Salt Lake City, UT, 2000.

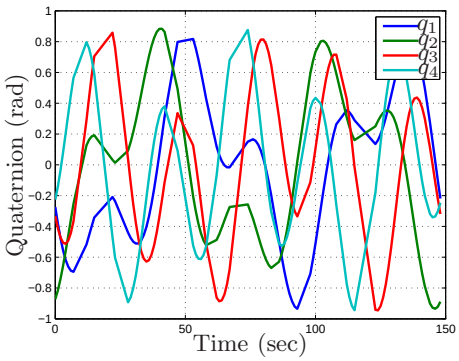

(a) Attitude (Deg)

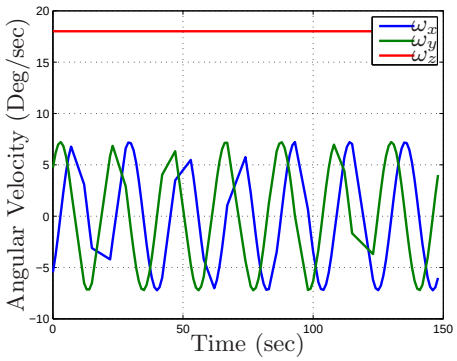

(b) Angular Velocity (Deg/sec)

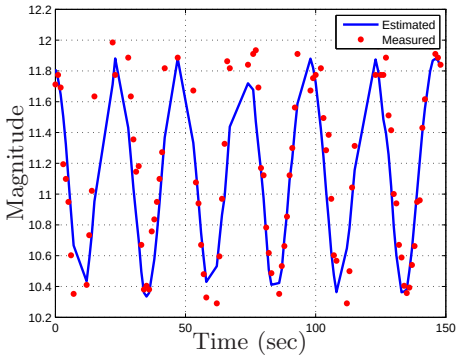

(c) Measure and Estimated Magnitude

Figure 10: Real Data Example